© 2021 Wiley-VCH GmbH

Supporting Information

for *Small,* DOI: 10.1002/smll.202103702

Integrated Assembly and Photopreservation of Topographical Micropatterns

*Shuailong Zhang, Weizhen Li, Mohamed Elsayed, Jiaxi Peng, Yujie Chen, Yanfeng Zhang, Yibo Zhang, Moein Shayegannia, Wenkun Dou, Tiancong Wang, Yu Sun, Nazir P. Kherani, Steven L. Neale, and Aaron R. Wheeler**

Supporting Information for

Integrated Assembly and Photopreservation of Topographical Micropatterns

Shuailong Zhang[1,2,3], Weizhen Li[4], Mohamed Elsayed[1,3], Jiaxi Peng[1,2,3], Yujie Chen[5], Yanfeng Zhang[5], Yibo Zhang[6], Moein Shayegannia,[6] Wenkun Dou,[7] Tiancong Wang,[7] Yu Sun,[3,6,7] Nazir P. Kherani[6,8], Steven L. Neale[4] and Aaron R. Wheeler[1,2,3,*]

1. *Donnelly Centre for Cellular and Biomolecular Research, University of Toronto, Toronto, ON, Canada M5S 3E1*
2. *Department of Chemistry, University of Toronto, Toronto, ON, Canada M5S 3H6*
3. *Institute of Biomedical Engineering, University of Toronto, Toronto, ON, Canada M5S 3G9*
4. *James Watt School of Engineering, University of Glasgow, Glasgow G12 8LT, UK*
5. *State Key Laboratory of Optoelectronic Materials and Technologies, School of Electronics and Information Technology, Sun Yat-sen University, Guangzhou 510275, China*
6. *Department of Electrical and Computer Engineering, University of Toronto, Toronto, ON, Canada M5S 3G4*
7. *Department of Mechanical and Industrial Engineering, University of Toronto, Toronto, M5S 3G8, Canada*
8. *Department of Materials Science and Engineering, University of Toronto, Toronto, ON, Canada M5S 3E4*

[*]Contact details for the corresponding author:

Aaron R. Wheeler; Email: aaron.wheeler@utoronto.ca; Tel: 416-946-3866; Fax: 416-946-3865

Address: Room 629A, 80 St. George Street, University of Toronto, Toronto, ON, Canada M5S 3H6

1. Projector for OET manipulation and UV photopolymerisation

In this work, we used a digital micromirror device (DMD) projector (Polygon DMD illuminator, Mightex Inc.) with two LED light sources (UV and red) to generate high-resolution light patterns on demand. The DMD projector is controlled by PolyScan software (Mightex Inc.), as shown in Figure S1. In practice, to generate light patterns for OET manipulation or UV photopolyermerisation, we load black and white images into the program, as shown in Figure S1(a). Then, when read, the user selects a particular image, the software shows the position and size of the image to be projected (using semi-transparent white image as an indicator), as shown in Figure S1(b). Finally, the user selects red or UV LED and presses "start", causing the given pattern to be projected onto the bottom plate of the OET device, with a video feed of the process available in the software, as shown in Figures S1(c) and S1(d), respectively. In addition, the power of the projected light patterns can be controlled via the software; in the work described here, we typically used 0.4 W/cm^2 for red light patterns and 0.3 W/cm^2 for UV light patterns.

There are several advantages of using Polygon DMD illuminator compared with previously-reported work of using standard data projectors[1-4]. First, the user-friendly PolyScan interface controls all aspects of operating the Polygon DMD illuminator to generate light patterns at different wavelengths on demand, making it possible for applications including not only OET manipulation but also UV photopolymerization. Second, the light patterns generated by the Polygon DMD illuminator have uniform optical power distribution. Third, the Polygon DMD illuminator is designed to be directly integrated with microscopes, significantly reducing the complexity of the OET system and minimizing the loss of optical power during light transmission.

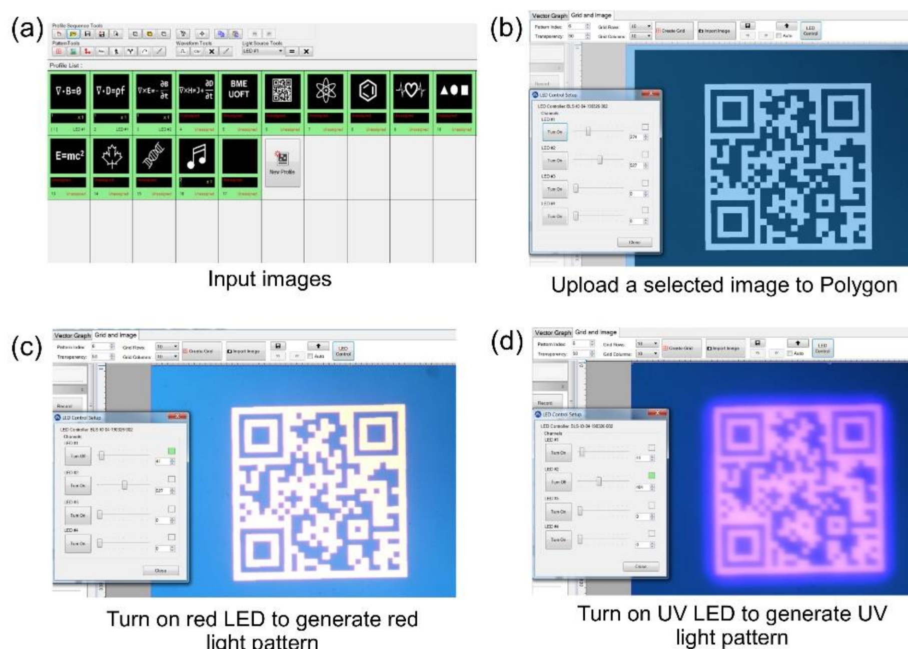

Figure S1. Screenshots from the Mightex PolyScan software interface illustrating the steps involved with forming light-driven patterns in an OET device. (a) Screenshot of a menu of custom black and white images that have been loaded into the program. (b) Screenshot illustrating the selection of a QR-code image. Screenshots illustrating the camera-view of the OET device under illumination by (c) red or (d) UV LED

2. Bottom-up assembled TMPs in cured hydrogel microstructures

Figure S2 features representative bright-field and fluorescent microscopy images of assembled/cured TMPs. These structures were prepared by bottom-up assembly from suspensions of carbon nanoparticles [Figure S2(a)-S2(d)], silver nanoparticles [Figure S2(e) and S2(f)], graphene nanoplatelets [Figure S2(g) and S2(h)], and fluorescent polystyrene microbeads [Figure S2(i)- S2(l)]. The noise levels in several of these images were characterized by evaluating pixel intensities. First, a blank hydrogel pattern formed from 1:4 diluted concentrated PEGDA was formed. A region of interest (ROI) in the center of the image was defined and the average grayscale value of pixel intensity was determined and recorded as $N0$. Then, for each image of a TMP to be evaluated, an ROI outside of the TMP was defined, and the average grayscale value of pixel intensity was determined for the ROI and recorded as $N1$. The relative noise in that image was then defined as $N = (N1 - N0)/N0$. In replicate measurements of different images for each particle type, we observe $N < 7\%$ for silver, carbon, and graphene nanoparticles and $N < 5\%$ for polystyrene microparticles. These levels were fine for the work described here, but in the future, noise might be reduced further by further optimization of bias voltage and frequency, projection-line-width, projection time, and composition of hydrogel mixture.

3. Scanning electron microscope images of nano-/micro- materials

Scanning electron microscope (SEM) images in this work were collected using an enviromental SEM (QUANTA FEG 250 ESEM) at the Centre for Nanostructure Imaging at the Department of Chemistry, University of Toronto. Under low pressure mode, the enviromental SEM allows direct imaging of non-conductive samples (such as polystyrene microparticles) without the need for coating their surfaces with conductive materials. The SEM images shown in Figure 1(k)-(m) in the main text and Figure S3(g)-(h) were

collected using an electron beam with 10 keV enegy and 3 nm spot size under a pressure of 130 Pa. The SEM images shown in Figure S3(a)-(f), (i)-(j) were collected using an electron beam with 5 keV energy and 3 nm spot size under a pressure of 5×10^{-4} Pa to 1.5×10^{-3} Pa.

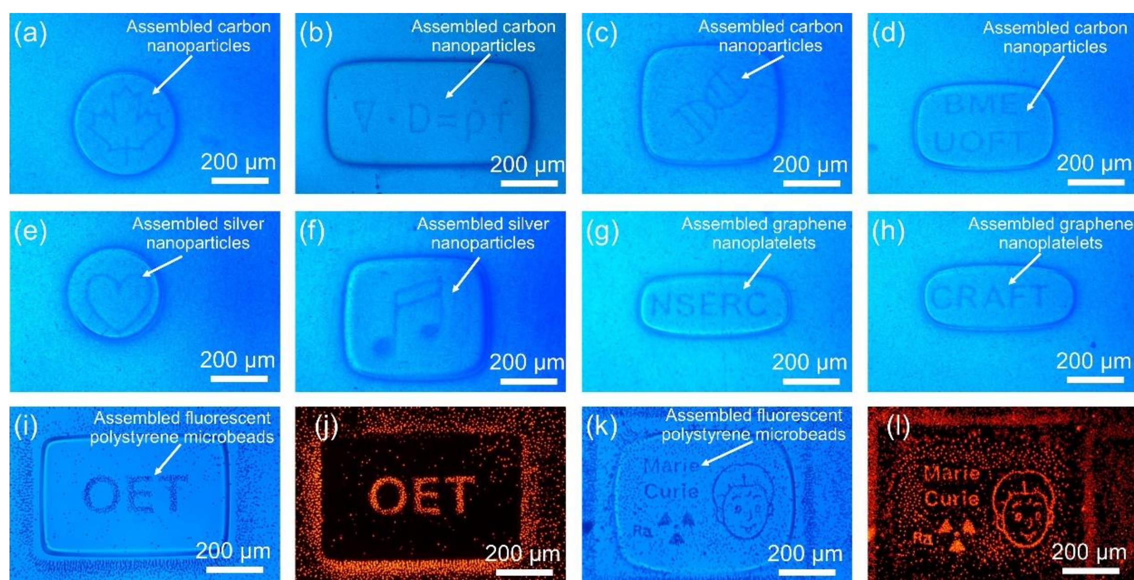

Figure S2. Bottom-up assembled/cured TMPs. Bright-field microscopy images of assembled/cured carbon nanoparticle TPMs depicting (a) a maple leaf and (b) the differential form of Gauss's Law, (c) the symbol for DNA, and (d) the text “BME UOFT” (abbreviation for biomedical engineering at the University of Toronto), assembled/cured silver nanoparticle TMPs depicting (e) a heart symbol, and (f) a symbol of music notes, and assembled/cured graphene nanoplatelet TMPs depicting (g) the text “NSERC” (abbrevation for the Natural Sciences and Engineering Research Council of Canada), and (h) the text “CRAFT” (abbreviation for the Centre for Research and Applications in Fluidic Technologies). Bright-field and fluorescence microscope images of assembled/cured 6 μm dia. poylstyrene microparticles depicting (i,j) the text “OET” (abbrevation for Optoelectronic Tweezers), and (k,l) a stylized caricature of Marie Curie with the symbol for radioactivity.

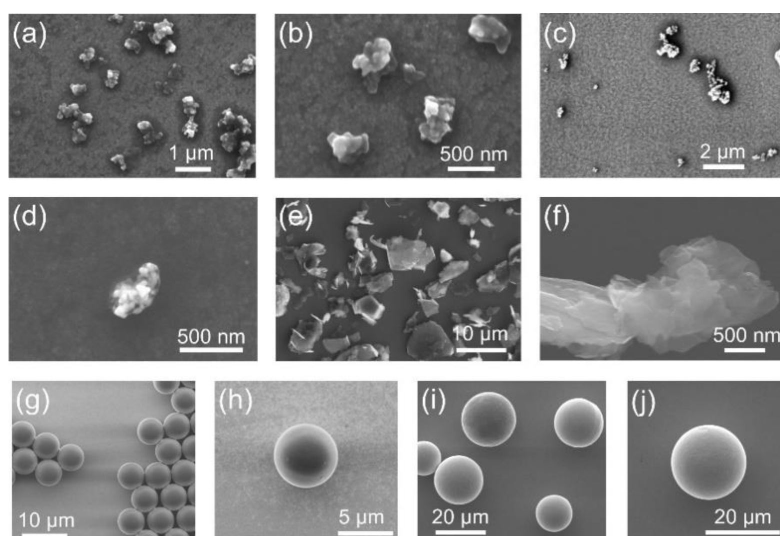

Figure S3. Micro-SEM images of (a,b) carbon nanoparticles, (c,d) silver nanoparticles, (e,f) graphene nanoplatelets, (g,h) polystyrene microbeads, and (i,j) solder microbeads. The samples are on ITO substrates.

4. Numerical simulations

3D simulations were generated in COMSOL Multiphysics using the AC/DC module (COMSOL Inc., Burlington, MA, accessed via license obtained through CMC Microsystems, Kingston, Canada). As shown in Figure S4, the model length (X-axis), width (Y-axis) and height (Z-axis) are set to 150 µm, 150 µm, and 150 µm, respectively. The bottom of the model represents an a-Si:H surface illuminated with a 30-µm-diameter circular light pattern in the center (purple region). A 20-µm-diameter solder bead is positioned at the left edge (on the X axis) of the circular light pattern (such that the center of the bead is 15 µm from the center of the light pattern), 100 nm above the a-Si:H surface (in the Z axis).

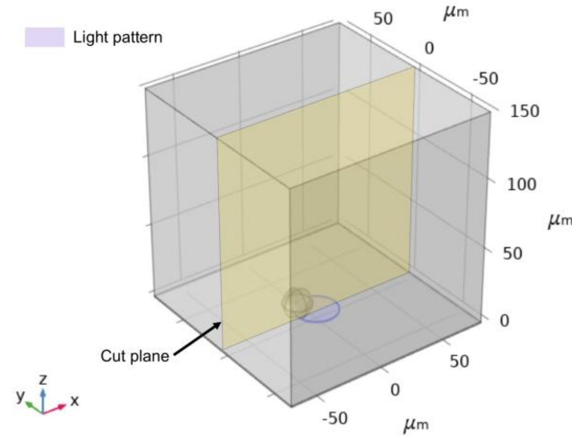

Figure S4. Sketch of the 3D simulation model. The XZ cut-plane (at Y = 0) shown in yellow was used for the simulations in Figure 5 in the main text.

In this model, the boundary conditions were set to electrical insulation at all external sides and electrical continuity for all interior boundaries. The initial electric potential was set to 0 V for all domains. Upon initiation of the simulation, the top and bottom surfaces were set to 15 V and 0 V to simulate the applied AC signal (with frequency set to 20 kHz). The model included a 1-µm-thick a-Si:H layer at the bottom and a 149-µm-thick liquid chamber. The conductivities σ and permittivities ε were set to $\sigma_{silicon_bright} = 5 \times 10^{-4}\ S/m$, $\sigma_{silicon_dark} = 1 \times 10^{-6}\ S/m$, $\varepsilon_{silicon} = 11.7$, $\sigma_{liq.\ medium} = 1.8 \times 10^{-2}\ S/m$, $\varepsilon_{liq.\ medium} = 80$, $\sigma_{solder} = 1 \times 10^{7}\ S/m$, $\varepsilon_{solder} = 1$. The model employed a free tetrahedral mesh with a maximum element size of 3.02 µm, a minimum element size of 0.0302 µm, a maximum element growth rate of 1.3, a curvature factor of 0.2, and a resolution of narrow regions of 1. Electric potential distribution and electric field distribution were simulated for the highlighted cut-plane in Figure S4 (XZ-slice at Y = 0 µm) and are shown in Figure 5(e)-(f) in the main text.

The model was then used to generate a numerical estimate of the DEP force experienced by the particle using the Maxwell stress tensor, as described previously.[5-8] Specifically, the DEP force can be simulated using the following equation (derived from Lorentz force law[5,6]):

$$F_{DEP} = \oint (T \cdot n) dS \#(1)$$

where S represents the surface enclosing the bead and n represents the unit vector. This methods takes the variation of electric field into account. To generate a full trap profile, the simulation was repeated by moving the solder bead center from X = -30 µm to X = +30 µm in increments with a step size of 0.5 µm. After generating

initial simulated results, they were normalized by dividing by a factor of 3 (this factor was determined empircally – e.g., the measured and initial-simulated forces for D = 13 μm were 265 and 789 pN, respectively), and were plotted in in Figure 5(c) in the main text.

5. Fabrication of metal contacts

Figue S5(a) shows the step-by-step fabrication process flow for forming metal contacts on OET bottom plates. Briefly, in a preparation step, an OET bottom plate was first cleaned by immersing in acetone for 5 minutes with agitation, then rinsed with isopropyl alcohol and deionized (DI) water, then air dried using pressurized nitrogen, and then baked at 100 °C for 5 minutes. In step 1, 2 mL SU-8-2005 (MicroChem) was spin-coated on top of the OET bottom plate (4000 rpm for 60 seconds), followed by soft baking at 95°C for 2 minutes. In step 2, a mask aligner (EVG 620) was used to illuminate the OET bottom plate (exposure energy: 100 mJ/cm^2) through a photomask to selectively photo-crosslink the SU-8. After post-exposure baking (95°C for 2 minutes) and developing in SU-8 developer (2 minutes), the OET bottom plate with SU8 structrures was rinsed with isopropyl alcohol, and then air dried with pressurized nitrogen followed by hard baking at 200 °C for 5 minutes. After completion of step 2, the a-Si:H on the bottom plate was mostly exposed, except for an array of sixteen isolated SU-8 features, each ~4 μm high. In step 3, 2 mL S1811 positive photoresist (MICROPOSIT) was spin-coated on the OET bottom plate with SU8 structures (3000 rpm for 30 seconds), followed by soft baking at 115°C for 1 minute. In step 4, the mask aligner (EVG 620) was used to expose the S1811 photoresist through an aligned photomask (exposure energy: 150 mJ/cm^2). After developing in MF319 developer for 1 minute, the OET bottom plate was rinsed with DI water and dried with pressurized nitrogen. After completion of step 4, the sixteen SU-8 features were exposed, while all areas around the SU-8 were covered in S1811. In step 5, a thin metal layer of Chromium/Au (10 nm/ 80 nm) was deposited on the OET bottom plate using an electron beam evaporator (home-made from components from Kurt J. Lesker; for Cr deposition: deposition rate 0.1 A/s, set point 5%; for Au deposition: deposition rate 1.2 A/s, set point 15.5%). In step 6, the metal-coated OET bottom plate was then immersed in a beaker of acetone to lift-off the the metal on the S1811 photoresist, leaving metal only on top of the SU-8 features. When complete, the bottom plate featured an array of sixteen electrodes, each insulated from the underlying a-Si:H by an SU-8 feature, as shown in Figure S5(b). Figure S5(c) shows an OET bottom plate with fabricated metal contacts and an OET top plate. The two plates were joined together with a 150-μm-thick spacer to form a chamber [Figure S5(d)], within which the solder beads were assembled in between the metal contacts. As shown in Figure S5(e), each pair of electrodes was separated by a gap of 100 μm. In some designs, each pair of electrodes was separated by a gap of 150 μm.

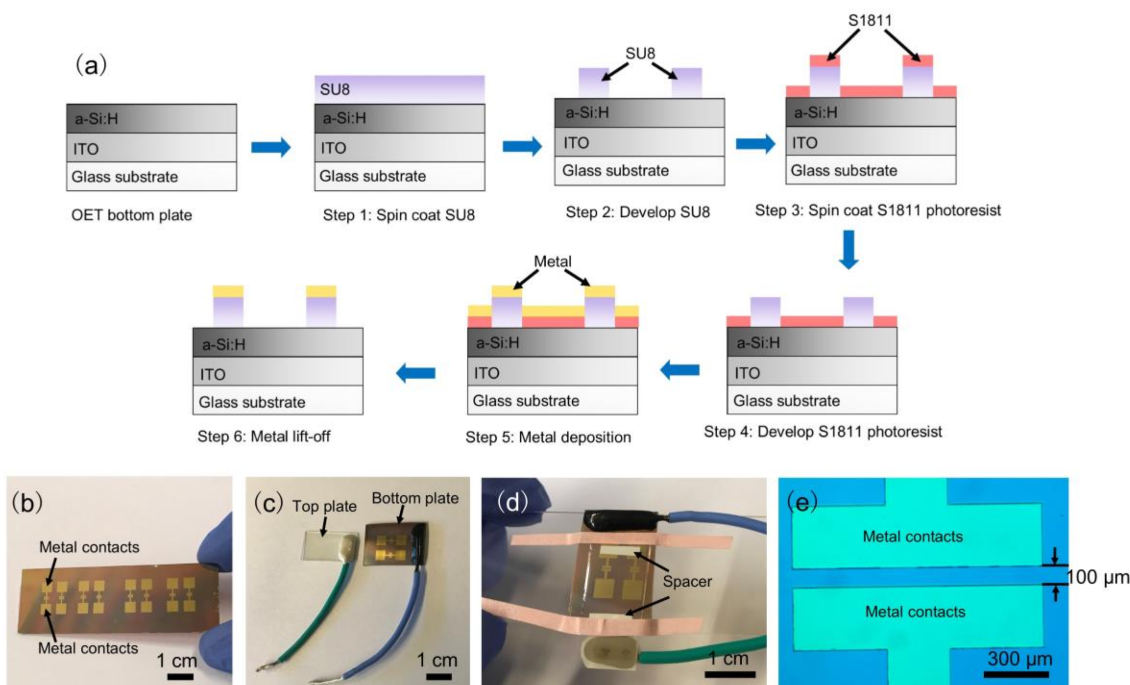

Figure S5. (a) Step-by-step fabrication process flow for forming isolated metal contacts on an OET bottom plate. (b) Image of an OET bottom plate after forming the metal contacts. (c) Picture of an OET bottom plate with metal contacts and an OET top plate. (d) Picture of an assembled OET device. (e) Bright-field microsocope image of the metal contacts (which appear in green colour) on an OET bottom plate (which appears as a blue colour).

6. Supplementary Movies

Movie S1. Using UV light patterns to form a cured hydrogel microstructures in the shapes of an outline of a maple leaf (clip 1), the mass-energy equation (clip 2), a triangle, circle, and square (clip 3), a quick response (QR) code (clip 4), a symbol of an atom (clip 5), and the chemical symbol for benzene (clip 6).

Movie S2. Using a doughnut-shaped light pattern to trap a single 10 μm polystyrene bead and move it at 14 μm/s in a solution with a ratio of 1:4 concentrated PEGDA to DI water.

Movie S3. Bottom-up OET assembly (with red light) of graphene nanoplatelets into a TMP of the chemical symbol for benzene (clip 1), carbon nanoparticles into a TMP of Gauss' Law for Magnetism (clip 2), and silver nanoparticles into a TMP of a stylized caricature of Albert Einstein with the mass energy equation (clip 3) (all in a solution with a ratio of 1:4 concentrated PEGDA to DI water), and preservation of the assmbled TMP of the chemical structure of benzene in a cured hydrogel microstructure using UV light (clip 4).

Movie S4. Translating a 20 μm dia. solder bead at 20 μm/s (clip 1) and 60 μm/s (clip 2) using a 30-μm-diameter circular light pattern in a solution with a ratio of 1:4 UV-curable hydrogel to DI water.

Movie S5. Assembly of five solder beads into a straignt line to connect two isolated metal contacts in a solution with a ratio of 1:4 UV-curable hydrogel to DI water.

Movie S6. Projecting a rectangular light pattern causes a microcapacitor to oscillate back and forth clip 1); projecting a positive/negative cage pattern allows translation of a microcapacitor at 30 μm/s (clip 2); rotating a positive/negative "cage" pattern allows at rotation of a microcapacitor at 6.2 deg/s (clip 3), all in a solution with a ratio of 1:4 UV-curable hydrogel to DI water.

Supplementary References

1. S. Zhang, Y. Liu, Y. Qian, W. Li, J. Juvert, P. Tian, J. C. Navarro, A. W. Clark, E. Gu, M. D. Dawson, J. M. Cooper, S. L. Neale, "Manufacturing with light - micro-assembly of opto-electronic microstructures", *Opt. Exp.* 25(23), 28838-28850 (2017).
2. S. Zhang, W. Li, M. Elsayed, P. Tian, A. W. Clark, A. R. Wheeler, S. L. Neale, Size-scaling effects for microparticles and cells manipulated by optoelectronic tweezers. *Opt. Lett.* 44, 4171-4174 (2019).
3. S. Zhang, E. Y. Scott, J. Singh, Y. Chen, Y. Zhang, M. Elsayed, M. D. Chamberlain, N. Shakiba, K. Adams, S. Yu, C. M. Morshead, P. W. Zandstra, A. R. Wheeler, The optoelectronic microrobot: A versatile toolbox for micromanipulation. *Proc. Natl. Acad. Sci. U.S.A.* 116, 14823-14828 (2019).
4. S. Zhang, N. Shakiba, Y. Chen, Y. Zhang, P. Tian, J. Singh, M. D. Chamberlain, M. Satkauskas, A. G. Flood, N. P. Kherani, S. Yu, P. W. Zandstra, A. R. Wheeler, "Patterned Optoelectronic Tweezers: A New Scheme for Selecting, Moving, and Storing Dielectric Particles and Cells", *Small* 14(45), 1803342 (2018).
5. X. Wang, X. B. Wang, P. R. C. Gascoyne, "General expressions for dielectrophoretic force and electrorotational torque derived using the Maxwell stress tensor method," *J. Electrostat.* 39(4), 277–295 (1997).
6. S. Kumar, P. J. Hesketh, "Interpretation of ac dielectrophoretic behavior of tin oxide nanobelts using Maxwell stress tensor approach modeling," *Sensor Actuat. B Chem.* 161(1), 1198–1208 (2012).
7. S. Zhang, A. Nikitina, Y. Chen, Y. Zhang, L. Liu, A. G. Flood, J. Juvert, M. D. Chamberlain, N. P. Kherani, S. L. Neale, A. R. Wheeler, "Escape from an optoelectronic tweezer trap: Experimental results and simulations", *Opt. Express* 26(5), 5300-5309 (2018).
8. S. Zhang, Y. Liu, J. Juvert, P. Tian, J. C. Navarro, J. M. Cooper, S.L. Neale, "Use of optoelectronic tweezers in manufacturing—accurate solder bead positioning", *Appl. Phys. Lett.* 109(22), 221110 (2016).